BBA - Bioenergetics 1861 (2020) 148240

Contents lists available at ScienceDirect

BBA - Bioenergetics

journal homepage: www.elsevier.com/locate/bbabio

Hydrogen bond network analysis reveals the pathway for the proton transfer in the E-channel of *T. thermophilus* Complex I

Umesh Khaniya[a,b], Chitrak Gupta[d,e], Xiuhong Cai[a,b], Junjun Mao[a], Divya Kaur[a,c], Yingying Zhang[a,b], Abhishek Singharoy[d,e], M.R. Gunner[a,b,c,*]

[a] Department of Physics, City College of New York, New York 10031, USA
[b] Department of Physics, The Graduate Center, City University of New York, New York 10016, USA
[c] Department of Chemistry, The Graduate Center, City University of New York, New York 10016, USA
[d] School of Molecular Sciences, Arizona State University, Tempe, AZ, USA
[e] Biodesign Institute, Arizona State University, Tempe, AZ, USA

ARTICLE INFO

Keywords:
Complex I
Proton pumping
Proton transfer
Hydrogen bond network
Grand Canonical Monte Carlo Simulations

ABSTRACT

Complex I, NADH-ubiquinone oxidoreductase, is the first enzyme in the mitochondrial and bacterial aerobic respiratory chain. It pumps four protons through four transiently open pathways from the high pH, negative, N-side of the membrane to the positive, P-side driven by the exergonic transfer of electrons from NADH to a quinone. Three protons transfer through subunits descended from antiporters, while the fourth, E-channel is unique. The path through the E-channel is determined by a network analysis of hydrogen bonded pathways obtained by Monte Carlo sampling of protonation states, polar hydrogen orientation and water occupancy. Input coordinates are derived from molecular dynamics trajectories comparing oxidized, reduced (dihydro) and no menaquinone-8 (MQ). A complex proton transfer path from the N- to the P-side is found consisting of six clusters of highly connected hydrogen-bonded residues. The network connectivity depends on the presence of quinone and its redox state, supporting a role for this cofactor in coupling electron and proton transfers. The N-side is more organized with MQ-bound complex I facilitating proton entry, while the P-side is more connected in the apo-protein, facilitating proton exit. Subunit Nqo8 forms the core of the E channel; Nqo4 provides the N-side entry, Nqo7 and then Nqo10 join the pathway in the middle, while Nqo11 contributes to the P-side exit.

1. Introduction

Complex I, the first protein in the aerobic electron transfer chain in bacteria and mitochondria, oxidizes NADH from the Krebs cycle to form a reduced quinone product [1–5]. The reduced, dihydro quinone (quinol) is then the substrate for the cytochrome bc_1 complex (complex III), which in turn produces a reduced cytochrome *c* substrate for cytochrome *c* oxidase (CcO, complex IV), where the terminal electron acceptor, O_2 is reduced [1]. Each of these proteins adds to the cellular energy of the transmembrane electrochemical gradient by removing protons from the high pH, N-side of the membrane and adding them to the low pH, P-side [3,6]. The resulting proton gradient, provides the fuel for the synthesis of ATP by complex V, which allows controlled movement of protons from P- to N-side, closing the mitochondrial electron and proton transport chain [1].

For proton pumps, such as complex I and CcO, protons move through the protein with energy provided by the redox reaction they catalyze. In complex I the redox chemistry and proton pumping are separated by a remarkable distance [7]. Thus, intramembrane channel opening and closing is tied to the redox chemistry which occurs in the long peripheral arm [1]. With the elucidation of an atomic resolution complex I structure [7] it is now possible to ask detailed questions about the mechanism by which the protein structure couples the energy releasing redox reactions with the energy storing proton transfer reactions.

A basic proton pump, that carries out a proton transfer process that is itself thermodynamically uphill, has several minimal requirements including [6]: (i) a change in proton affinity during the reaction cycle so protons will be bound from the N-side and released to the P-side via transiently loaded sites in the protein interior; (ii) a pathway for protons to be handed from donor to acceptor through the hydrophobic interior of the membrane embedded region of the protein via a Grotthuss mechanism [8]; (iii) a means to close off proton transport so that the interior is only accessible to the N-side during proton uptake into

* Corresponding author at: Department of Physics, City College of New York, New York 10031, USA.
E-mail address: mgunner@ccny.cuny.edu (M.R. Gunner).

https://doi.org/10.1016/j.bbabio.2020.148240
Received 29 December 2019; Received in revised form 19 May 2020; Accepted 3 June 2020
Available online 09 June 2020

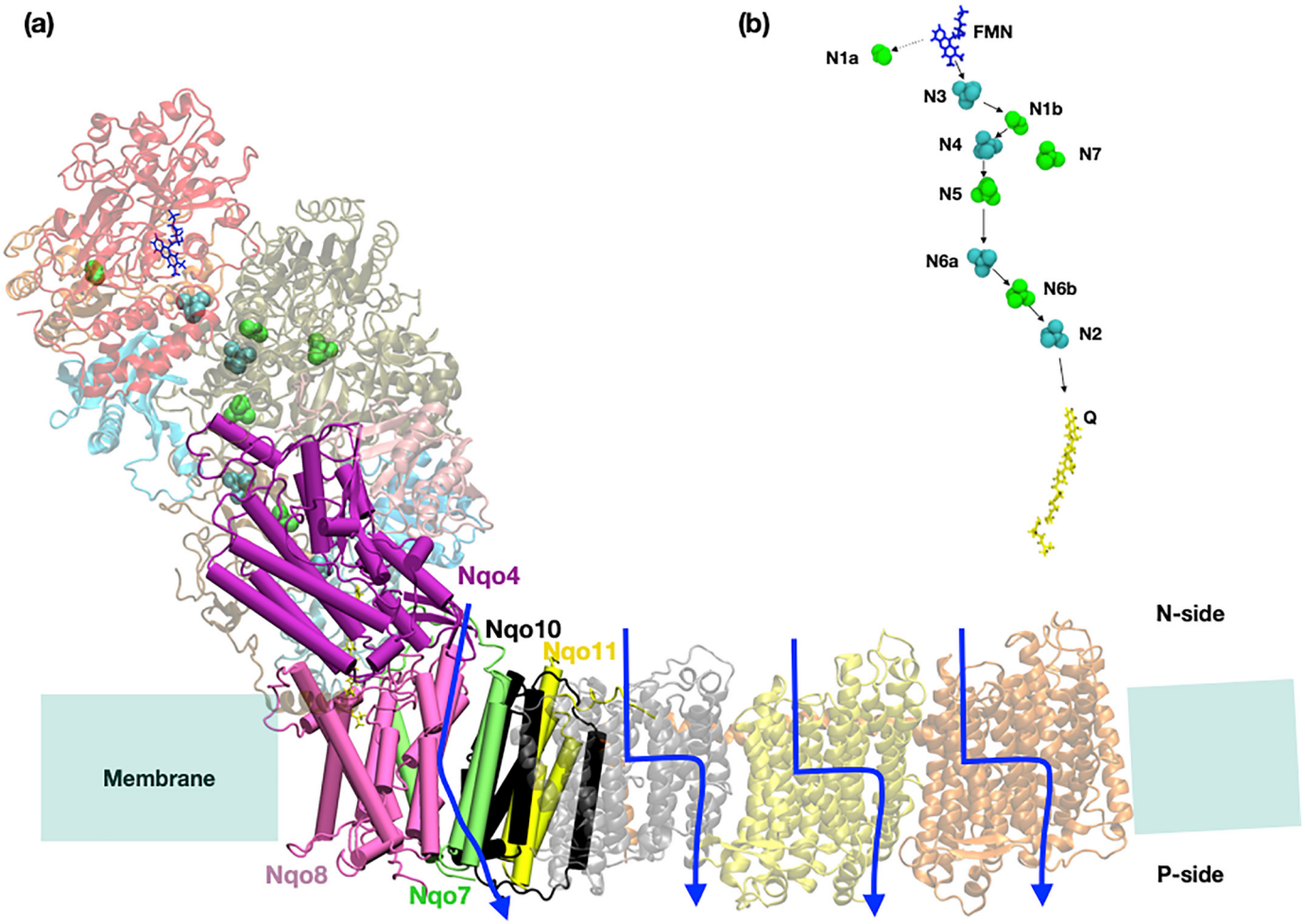

Fig. 1. *T. thermophilus* complex I. (a) Subunit Nqo4, Nqo7, Nqo8, Nqo10, and Nqo11, which are studied here, are shown as solid cylinders. The antiporter subunits Nqo12, Nqo13 and Nqo14 are shown as semi-transparent ribbons. Iron sulfur clusters are shown in green (oxidized) and cyan (reduced). Blue arrows show direction and approximate position of proton pumping paths. (b) Cofactors in the peripheral arm. Iron-sulfur clusters that are reduced in the MD trajectory are cyan while the rest are green. FMN is shown in blue and menaquinone-8 in yellow. Black arrow represents likely path for electron transfer after NADH has reduced FMN. NADH is not shown.

the protein and accessible to the P-side during release to keep protons from moving downhill. Here, the pathway and its control elements are investigated for complex I [7], using computational approaches that we have developed for related protein pumps such as cytochrome *c* oxidase [9].

Mitochondrial complex I has up to forty-five subunits including fourteen core subunits that are highly conserved from bacteria to humans [7,10–14]. The latest complete crystal structure of complex I was solved at 3.3 Å from the smaller, bacterial *Thermus thermophilus* [7], which maintains the peripheral subunits for the redox reactions and intra-membrane proton pumping subunits, but lacks smaller regulatory subunits found in higher organisms [13]. It may thus provide a more direct look at the minimum requirements for pumping. The peripheral arm, containing all the redox cofactors, extends 140 Å into the P-side of the membrane, while the intramembrane subunits is 180 Å long (Fig. 1) [15]. Soluble NADH is bound at the end of the peripheral arm furthest from the membrane. Electron transfers from NADH reduce quinone via non-exchangeable FMN and iron-sulfur complexes. The quinone, which is the terminal electron acceptor, enters from the membrane and snorkels up through the protein to the binding site (Fig. 1) [16]. The quinone position in the complex I is unique as the hydrophobic cofactor must move 25–30 Å above the membrane surface [7]. In the other quinone requiring proteins the binding site is within the membrane plane. The electron transfer reaction is tightly coupled to pumping of four protons [1,17,18].The protons move through four separate, transiently opened, hydrated pathways in the membrane domain (Fig. 1). The overall reaction is:

$$NADH + H^+ + Q + 4H_N^+ \rightarrow NAD^+ + QH_2 + 4H_P^+$$

There are seven subunits in the membrane domain of *T. thermophilus* complex I [7]. Three protons are pumped through the three homologous antiporter subunits, denoted Nqo12, Nqo13, Nqo14 (Fig. 1). While the protein interior is largely made up of hydrophobic residues there are groups of ionizable residues (Asp, Glu and Lys) that were identified as possible proton pathways through these subunits from the structure [7,13,19] which were largely confirmed by site-directed mutagenesis [20–22]. The X-ray crystal structure of complex I has provided the starting information needed for in depth analysis of the potential proton pumping pathways. These studies have generally used Molecular Dynamics (MD) simulations to trace out hydrogen bonded pathways in trajectories obtained with different protonation states of buried residues or redox states of cofactors [23–26] and Hybrid Quantum Mechanics/Molecular Mechanics (QM/MM-MD) to investigate very local proton transfer events [23,25,26]. MD simulations carried out with the membrane domain of *E. coli* showed that protonation state changes of key Glu and Lys in the center of the protein change the hydration of channels that can support proton transfer [23,24]. The results of MD simulation using the complex I structure

generally supported the pathways predicted given the location of buried charged and polar residues in the crystal structure [25,26]. The local barriers to hydronium migration from N to P side with nearby residues in different protein protonation states were examined in the antiporter subunits by hybrid computational methods combining QM/MM and MD [23,25,26].

Complex I is clearly the result of evolution repurposing different proteins for new functions: the peripheral arm of complex I is derived from the soluble [NiFe] hydrogenases [27,28], whereas the antiporter subunits of the membrane arm are derived from Mrp cation/H^+ antiporters [29]. The intramembrane subunit, Nqo8 connects to the peripheral arm. It is the most conserved subunit in complex I [1], however it appears not to be related to other proteins.

While there are three antiporter derived subunits, four proton are pumped [17]. Thus the sequence and structure of the fourth channel is unique [1]. The crystal structures [13,19] led to the suggestion that the fourth channel may use subunits Nqo10 and Nqo11 (NuoJ/K in *E. coli*), an assignment which was also supported by MD simulations carried out on the *E. coli* protein [23]. However, after the structure of the *T. thermophilus* complex I was solved [7], it was suggested that Nqo8 forms the fourth channel, now called the E-channel due to the abundance of glutamic acids in this proposed path [7]. Recent QM/MM-MD simulations using the *T. thermophilus* complex I identified a path entering from the N-side to central residues Glu213/163 of the Nqo8 subunit [26] or via the interface between Nqo10 and Nqo11 [25]. Several internal resides have been suggested as important include 7(Asp72), Glu130, Glu163, Glu213, 10(Tyr59) and 11(Glu32) [7,19,23,25,26] (the nomenclature is subunit(residue). Subunit Nqo8 is not explicitly stated). However, the P-side proton exit has not been identified. Recent work suggested that reduction of quinone triggers movement of the cofactor to be closer to the membrane domain which is coupled to changes in the protonation of residues around quinone position [30,31].

Hydrogen bond networks that can support proton transfers can be identified using a number of computational methods. MD trajectories allow for the protein to move freely within a membrane, with waters moving in and out. However, the protonation states are predefined. In contrast, Monte Carlo (MC) techniques allow for sampling of sidechains protonation and position as well as the occupancy and orientation of waters with the restriction of a fixed backbone [32]. This allows for dynamic sampling of protonation states, while incurring restrictions on the movement of the protein [9,33]. Constant pH MD (cpHMD) allows protonation states to change within a MD trajectory [34–36]. Despite a handful of successes [37], it is not yet able to bring a large system with many interacting protonatable groups to equilibrium so is not a good tool for analysis of complex I. Currently methods that carry out MC analysis on snapshots generated by MD (MD/MC) provides a reasonable compromise, especially if the MD snapshots can credibly capture biologically relevant conformational states [9].

An MC analysis of hydrogen bond networks in MD trajectories has been employed to identify the exit pathway for protons from *Rb. sphaeroides* cytochrome *c* oxidase [9]. Polar and ionizable amino acid side chains were identified as participating in proton transfer via buried waters. Highly connected hydrogen-bonded residues were identified as clusters of 6–22 residues where all residues are connected to multiple residues in the cluster either directly or via short water chains. Thus, the model did not support a set of simple linear proton transfers. Rather protons appear to be able to move easily within clusters. An excess, pumped proton can be transiently trapped within an individual cluster, with a distribution that reflects the relative proton affinity of sites within the complex environment [38]. In cytochrome *c* oxidase gating of proton transfer occurs when inter-cluster connections are broken, usually by loss of connecting waters [38–40].

Here, we perform an MD/MC network analysis of hydrogen bonds derived from MC calculations of MD snapshots carried out with the most recent complex I structure from *T. thermophilus* [41]. The simulations are carried out using trajectories with the oxidized menaquinone-8, MQ, the reduced MQH_2, and with no quinone (the apoprotein). Monte-Carlo analysis of the hydrogen bond network was performed across five protein subunits at the junction between the soluble and the transmembrane domains of complex I (Nqo4, Nqo7, Nqo8, Nqo10, and Nqo11 (Fig. 1)) to identify the E-channel proton pathway. A complete proton transfer pathway is found between the N and the P-sides of the membrane. Comparing the connections in states with different quinone occupancy it is shown that connections to the N-side are strong in the quinone containing protein, while the P-side is more connected in the apo-structure, providing a possible gating mechanism to control access to the different sides of the membrane.

2. Methods

2.1. MD simulation

Models employed in our MC simulations are extracted from our recently reported MD simulations of the *T. thermophilus* complex I [41]. Preparation of the simulation system is described in the MD article, and summarized herein. The initial complex I model was derived from the 3.3 Å crystal structure (PDB ID: 4HEA). Loops within the Nqo6 subunit between residues 55–70 were reconstructed using the more recent decyl ubiquinone-bound complex I structure [PDB ID: 6I0D]. In subunits Nqo7, 8, 12–14 all the Asp, Glu, Arg and Lys were considered to be ionized and His are modeled as neutral with the proton on NE. The complete molecular model (complex I embedded in a hydrated patch of 1000 1-palmitoyl-2-oleyol-sn-glycerophosphocholines [POPC] in the presence of 150 mM NaCl) consisted of ~1,000,000 atoms in a box of 28 nm × 14 nm × 24 nm. This system was parameterized with the CHARMM36 force field, including CMAP corrections for proteins [42,43]. The TIP3P model was employed to describe explicit water interactions. CHARMM parameters for the Iron-sulfur cluster were derived by Chang and Kim from Density Functional Theory calculations [44]. Clusters N1a, N1b, N5, N7 and N6b were oxidized and N3, N4 N6a and N2 reduced, preserving an alternation of oxidized and reduced states [2]. This pattern is supported by studies on bovine complex I [45–47]. It has been shown that N1a in *T. thermophilus* is not NADH-reducible, akin to bovine complex I [48,49]. The Flavin mononucleotide was described with the parameter set designed by Freddolino et al. [50].

The polar ring of menaquinone was aligned with that of decyl-ubiquinone in the X-ray structure (PDB ID: 6I0D), so the phenyl oxygens are interacting with residues His 38 and Tyr 87 of subunit Nqo4. The menaquinone tail was then refined using 10 ns of Molecular Dynamics Flexible Fitting (MDFF) [51] simulations into the hollow quinone-binding cavity. The structure with the highest cross-correlation and lowest energy was chosen for subsequent MD simulation. The system was equilibrated in the *NPT* ensemble (T = 313 K, P = 1 atm for 100 ns) before initiating production runs. Simulations were performed using 1.0 fs timestep with a force-based switching function for long-range interactions from 10 to 12 Å, Langevin thermostat, Nosé-Hoover Langevin barostat, and a flexible cell. Trajectories were run for 0.5 μs. Eighteen snapshots were taken from one trajectory of the apo-protein and the protein with MQH_2 or MQ bound. Eleven snapshots were obtained from a second trajectory with MQ bound. Snapshots were selected to have different levels of hydration (Fig. SI.1).

2.2. MCCE simulation

The hydrogen bond networks are obtained with MC sampling of multiple MD snapshots [9] using MCCE [33]. Only subunits Nqo4, Nqo7, Nqo8, Nqo10, and Nqo11 are included. As MCCE maintains a rigid backbone there is little interaction with subunits further away. The protein is inserted into a 33 Å thick rectangular slab using IPECE to emulate the membrane [52]. IPECE embeds the protein in a low dielectric slab so that the fewest surface ionizable residues are buried by

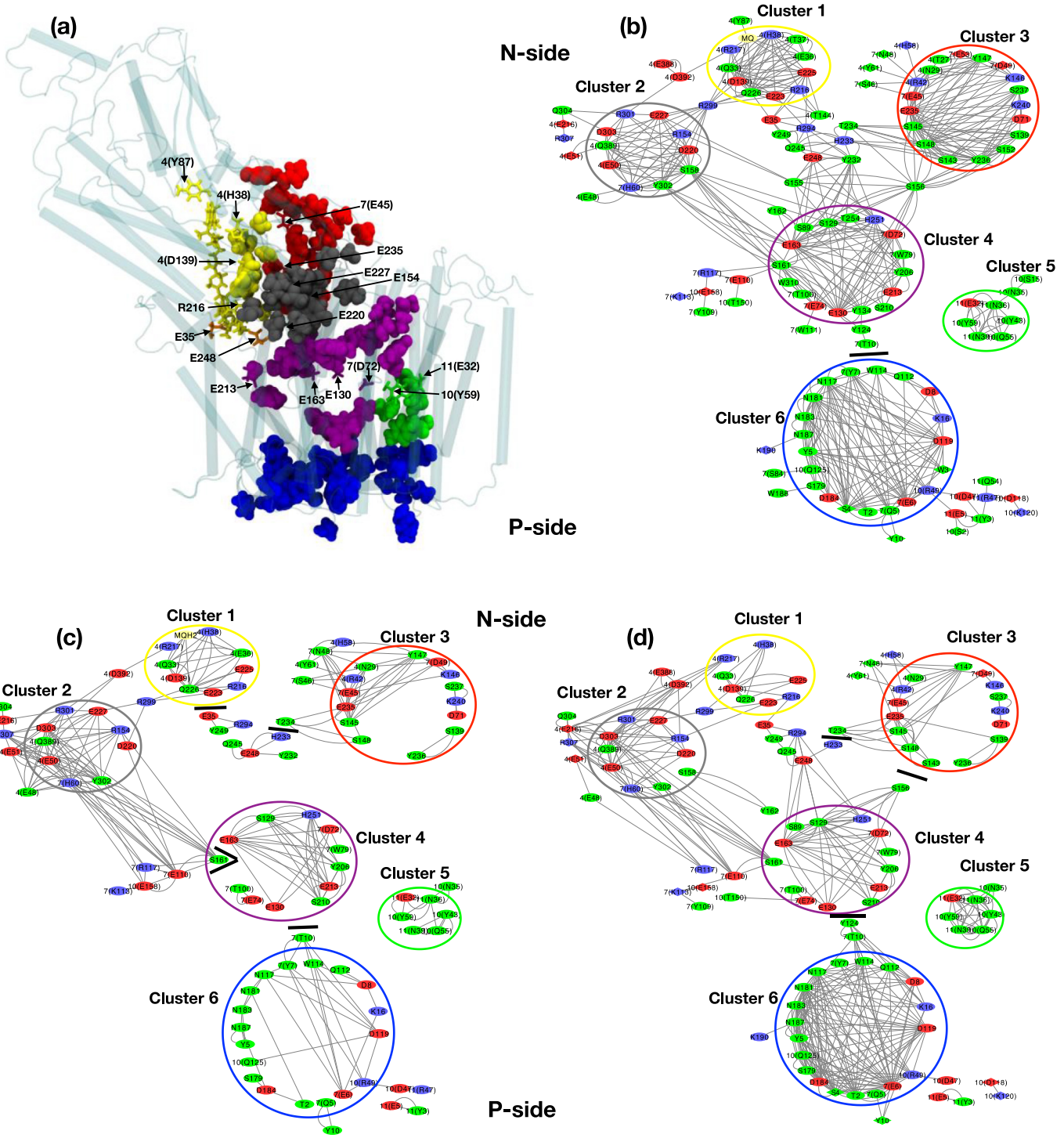

Fig. 2. Hydrogen bond networks for complex I E channel. (a) Subunits Nqo4, Nqo7, Nqo8, Nqo10, and Nqo11 are shown as semi-transparent cylinders. Side chains identified with each cluster: 1: yellow, 2: gray, 3: red, 4: purple, 5: green, 6: blue. Several key residues are labeled. (b, c, d) MCCE hydrogen bond network for: (b) the menaquinone docked structure; (c) the reduced menaquinone (MQH_2) docked structure; (d) without menaquinone. Clusters of highly connected residues are placed within a circle with the color used in the adjacent structure. A line represents residues connected by zero to four waters. Prefix in each node is subunit number. Residues from Nqo8, which contributes the most residues, do not have a prefix. One letter amino acid code is followed by the residue number. The node color is based on the residues type. Acid: red; base: blue; polar: green; MQ or MQH_2: yellow; diamond nodes: surface residues. All residues are enumerated in Table 1. The node labels can be read when the PDF image is magnified and an enlarged figure is found in Fig. SI.6. The positions of nodes are initially fixed with the analysis of the MQ containing structures, which is the most highly connected. Breaks in connections between nodes that are close together in the MQH_2 or quinone removed trajectories are made more visible by short black lines.

calculating the exposed surface area of Asp OD1 and OD2, Glu OE1 and OE2, Arg NH1 and NH2, and Lys NZ. Surface water molecules with > 5% solvent accessible surface are replaced with continuum solvent.

In MCCE a conformer represents a choice (degree of freedom) for a side chain or ligand or water that is available for Monte Carlo (MC) sampling [33]. Here, the protein backbone and side chain carbon atoms are obtained from the input MD snapshot and held fixed in MCCE. Multiple 'isosteric' conformers that change the position of polar hydrogens of side chain and water polar protons, the protonation state of Asp, Glu, Arg, Lys, Tyr and Cys and the occupancy of water binding sites are sampled [33]. This allows extensive analysis of the allowed hydrogen bond network for individual snapshots obtained from MD trajectories.

All buried waters are allowed to remain as they are essential members of hydrogen transfer pathways. The oxygen of each buried water oxygen generates 5 to 100 conformers with different proton positions. Each water also has a conformer moved into solution. MCCE uses GCMC (Grand Canonical Monte Carlo) sampling, which allows the number of water molecules within the complex to change by keeping constant chemical potential, volume and temperature of a reservoir. The behavior of TIP3 water in GCMC sampling in MCCE has been recently benchmarked against the behavior of water in MD [53]. In calculations that enhance hydration, a different function in the IPECE program inserts water oxygens into cavities that can accommodate a sphere with a radius of 1.4 Å [52].

At least 11 MD snapshots were subjected to MC sampling, collecting 17 to 35 million microstates for each snapshot. Thus, MCCE samples as many microstates as the timesteps that are needed to obtain more than a 10 ns MD trajectory. The MC analysis can reveal the complexity of the possible network connections. The network for each snapshot is formed from the hydrogen bonds found in at least 0.1% of microstates in the Boltzmann distribution. In the default network analysis, two residues or ligands are viewed as being connected if they can be bridged by zero to 4 water molecules. A permissive network is built up here as it contains connections from different microstates in a single snapshot. In addition, in the default presentation, networks from different snapshots from the same trajectory are merged. Networks are visualized using Cytoscape [54]. Additional description of the hydrogen bond network criteria is given in Table SI.1.

Active proton transfer networks end at the surface of the protein. Surface residues are identified based on their solvent accessible surface in the first frame of the menaquinone bound snapshot. A residue is considered surface exposed if 20% of the whole residue is surface exposed.

Conservation of a residues is determined by HSSP multiple alignment of approximately 2500 sequences of complex I [55].

3. Results and Discussion

The aim of this paper is to identify the proton transfer pathway in the unique E-channel of complex I, and to observe whether the connectivity of the path is influenced by the presence of an oxidized or reduced MQ or absence of MQ in a manner that might be able to control proton transfer across the membrane. MC sampling is performed on multiple MD snapshots to determine the Boltzmann distribution of ionization states, water occupancy and the resultant hydrogen bonded connections that can carry protons [9]. While the entire protein was contained in the MD trajectory, only subunits Nqo4, Nqo7, Nqo8, Nqo10, and Nqo11, which are distinct from the antiporter-derived subunits are included in the MC analysis (Fig. 1). The quinone is not present in this crystal structure. Recent papers have described several possible positions for the quinone in *T. thermophilus* [30,31]. Here MQ was aligned starting from the structure with decyl-DQ bound (PDB ID: 6I0D) where the introduced MQ carbonyls bound via 4(Tyr87) and 4(His38).

Simulations started with snapshots from the MD trajectory with bound MQ-8 generate the most complete pathway from N- to P-side of the protein. This will be described first and then compared with the results from trajectories with reduced or no quinone. The resultant analysis of the hydrogen bonds between amino acids, allowing for intervening waters does not produce a linear pathway. Rather, it shows a complex cluster of interconnections. This complexity is illustrated in several ways. Fig. 2a shows the amino acid side chains that are identified as making up the network of residues that can connect the N- to P-side of the protein. They are colored to represent clusters identified by the network analysis shown in Fig. 2b, where residues are divided into 'clusters' and 'connecting residues.'

In the network, a connection, represented by a line (edge), indicates a hydrogen bond path between the two residues (nodes). A connection can be direct or through as many as 4 intervening waters, and must be found in at least 0.1% of the accepted MC microstates found in MCCE simulations on at least one MD snapshot [9]. A cluster is made up of residues that each have connections to three or more other residues within that cluster (Fig. 2b–d). Our working hypothesis is that protons can move freely within a cluster, with the proton distribution determined by the relative residue proton affinity of individual sites [38,56]. Given the distribution of connections found by MC sampling of available hydrogen bonds and the branching of connections allowed by bridging waters, residues are found to be connected to as many as 18 other intra-cluster and inter-cluster residues. Peripheral nodes, shown outside the highly connected ring, are connected to only one or 2 other residues. Peripheral residues are counted as part of the cluster in Tables 1 and 2. Six highly connected clusters are identified. Connecting

Table 1
Residues in each cluster.

	Residues in cluster or connectors	Subunits Nqo
Cluster 1	4(Q33), 4(S36), 4(T37), 4(H38), 4(D139), 4(R217), R216, E223, E225, Q226, {4(Y87)}	4, 8
Cluster 2	4(E50), 4(Q389), 7(H60), R154, S158, D220, E227, R301, Y302, D303, {4(S48), 4(E51), 4(E216), Q304, R307)}	4, (7), 8
Connecting 1and 2	4(E388), 4(D392), R299	4, 8
Cluster 3	4(T27), 4(N29), 4(R42), 7(E45), 7(D49), 7(E53), D71, S139, S143, S145, K146, Y147, S148, S152, E235, Y236, S237, K240, {4(H58), 4(Y61), 7(S46), 7(N48)}	4, 7, 8
Cluster 4	7(T10), 7(D72), 7(E74), 7(W79), 7(T100), 7(W111), S89, Y124, S129, E130, Y134, S161, Y162, E163, Y206, S210, E213, H251, T254, W310, {7(Y109), 7(E110), 7(K113), 7(R117), 10(T150), 10(E158)}	7, 8, 10
Connecting 1, 2, 3 and 4	4(T144), E35, S155, S156, Y232, H233, T234, Q245, E248, Y249, R294	8, (4)
Cluster 5	10(Y43), 10(Q55), 10(Y59), 11(E32), 11(N36), 11(N39), {10(S15), $10(N35_{10})$}	10, 11
Cluster 6	7(Q5) 7(E6), 7(Y7), 7(S84), T2, W3, S4, Y5, D8, K16, Q112, W114, N117, D119, S179, N181, N183, D184, N187, W188, K190, 10(R49), 10(Q125), {Y10, 10(S2), 10(E5), 10(D47), 10(D118), 10(K120), 11(Y3), 11(R47), 11(Q54)}	7, 8, 10, 11

Residues in each cluster from *T. thermophilus* complex I (PDB ID: 4HEA). Residues from Nqo8, which contributes the most residues, do not have a prefix. The other subunits included in the analysis (Nqo4, 7, 10 and 11) are identified by the prefix number. Residues inside curly brackets are peripheral residues, on the edge of the cluster, connected to only one or two cluster residues. Underlined residues are surface exposed (%SAS ≥ 20) identified using MCCE on the first frame of the menaquinone bound snapshot. Subunits Nqo column: The subunit that contributes residues to each cluster. Subunits in parenthesis contribute only one residue to the cluster. The designation of these subunits in other organisms is found in [58].

Table 2
Count of residue types within each cluster.

Cluster	Count of residues in network obtained from MQ containing trajectory				
	Total	Acid (D, E)	Base (K,R)	Grotthuss polar (S, T, Y, H)	Non-Grotthuss polar (Q,N,W)
Cluster 1	11	3	2	4	2
Cluster 2	15	6	3	4	2
Connecting clusters 1–2	3	2	1	0	0
Cluster 3	22	5	3	12	2
Cluster 4	26	7	2	14	3
Connecting clusters 1–4	11	2	1	7	1
Cluster 5	8	1	0	3	4
Cluster 6	32	7	5	9	11
Total residues in clusters	128	33	17	50	24
Total residue in studied system	390	94	78	161	57

Number of residues in each cluster, including peripheral residues the cluster edge (Table 1). Total residue counts all residues in subunits Nqo4, Nqo7, Nqo8, Nqo10, and Nqo11which can form hydrogen bonds. Grotthuss competent polar residues have a lone pair and a polar proton so can accept and donate a proton. These are hydroxyl containing side chains Ser, Thr and Tyr, as well as His, Glu and Asp, which are Grotthuss competent when neutral.

residues bridge clusters. The network figure shows each residue name, which can be read when the image is magnified (Fig. SI.6). All residues in the network are also listed in Table 1.

Another measure of the complexity of the network can be seen in how many residues are included. Here 128, mostly buried residues within three transmembrane subunits of complex I are involved in the network (Table 2). This group of residues can be divided into several categories that define their possible functions. Grotthuss-competent residues can participate in Grotthuss proton transfer as they have a lone pair of electrons that can accept a proton as well as a dissociable proton. Water molecules, hydroxyl containing side chains, protonated acidic residues and neutral His meet these criteria. Non-Grotthuss residues can make strong hydrogen bonds but are not set up to 'simultaneously' receive and release a proton. A neutral Lys can serve, but an ionized Lys has no lone pair to accept a proton. Likewise, an Arg can only facilitate proton transfer if it (initially) loses a proton, which must be replaced on the same nitrogen [57]. Non-Grotthuss side chains can anchor the network and will strongly influence the proton affinity of residues within and near the cluster.

The network shown in Fig. 2b identifies an almost complete path between the N and P-side when MQ is bound. Overall, we see two clusters (2 and 3) which have residues that connect to the N-side of the membrane. They surround the quinone containing cluster (1). Clusters 1,2, and 3 connect to the deeply buried cluster 4. A small isolated cluster (5) is also found. Cluster 6 contains P-side surface exposed residues. With MQ bound there is a gap between clusters 4 and 6, which can stop proton flow.

3.1. Character of the clusters that make up the E-pathway in the MQ containing structures

The aim here is to provide specific detail for the E-pathway residues in each cluster in the MQ trajectory. The proton pathway we will describe reaches from the quinone binding site to exits on the P-side. Here we will describe the makeup of the clusters and the inter cluster connections.

Cluster 1 (11 residues) and 2 (15 residues) are near the N-side of the protein with 3 surface exposed residues in cluster 2 (Tables 1 and 2). Cluster 1 is linked directly to the quinone via 4(Tyr87) and 4(His38) without intervening waters (Fig. SI.2). These two clusters are internally highly connected. For example, four residues in cluster 1 are connected in some microstates to more than six other cluster 1 resides. The ionizable residues in cluster 1 and 2 are highly conserved (Table SI.6). Site-directed mutations have shown cluster residues 4(Tyr87) and 4(His38) [59,60] and Arg216 [61] and 4(Asp139) [62] in cluster 1 and Glu220, Glu227 and Arg154 in cluster 2 [61] decrease the quinone dependent activity. Recent simulations also show a role for 4(His38) in quinone binding [63].

Fig. 2 shows connections that are present in the MCCE network analysis of at least one snapshot. Cluster 1 and 2 are interconnected by two residues and connected to cluster 3 and 4 via multiple residues (Table 1 and Fig. 2(b)). Table SI.2 shows how many snapshots show the connections. Cluster 1 is connected to cluster 2 in 100% of the individual snapshots; to cluster 4 in 67% of the snapshots; and to cluster 3 in only 6% (1 of 18) snapshots (Table SI.2).

The large cluster 3 has 22 residues, with seven surface exposed providing entry to the interior (Table 1). Cluster residues 7(Glu45) and Glu235 have been shown to help support quinone dependent activity [12,19]. This cluster makes rare connections to the quinone binding cluster 1 and to the fully buried, central cluster 4 via Ser156 and Thr234 (Table SI.2).

Cluster 4 sits in the middle of the protein and is connected to clusters 1 (95%), 2 (28%) and 3 (6%) towards the N-side and comes close to cluster 6, which is the P-side exit. The numbers in parenthesis show the number of MD snapshots where the clusters are connected (Table SI.2). Previous inspection of the structure [7] led to the suggestion that residues in cluster 4, including 7(Asp72), Glu130, Glu163, Glu213, could play a role in forming the E channel. The crystal structures of the *T. thermophilus* Complex I includes no water molecules. Previous MD studies showed that the central cluster region undergoes a large increase in hydration which depends on the residue ionization state [26], which helps proton uptake from the N-side into what is denoted cluster 4 here [62]. The residues in cluster 4 are highly conserved (Table SI.6).

Cluster 5 has only eight residues, which are highly conserved. These include 10(Tyr59) and 11(Glu32) which have been previously suggested to play a role in the proton transfer pathway (Table 1 and Fig. 2b) [12,19]. The cluster has a high proportion of direct sidechain connections and hence is not significantly changed when the hydrogen bond analysis does not consider bridging waters, which makes it more visible in a direct inspection of the structure (Fig. SI.2). However, it is never connected to any other clusters in any of our standard MCCE analysis of MD snapshots.

The network analysis finds cluster 6 on the P-side made up of 32 residues, including eight highly conserved surface residues (Tables 1 and SI.6). Only cluster 6 has residues exposed to the P-side of the protein, so it must connect to one of the internal clusters (4 or 5) to allow for proton release. Despite cluster 6 being internally highly connected, we find no connection between cluster 6 and 4 or 5 in the snapshots derived from the MQ containing trajectory. Thus, a region that can provide a clear gate to stop proton transfer is at this junction. We will return to the completion of the network following the comparison of the MQ, MQH_2 and apo trajectories.

3.1.1. Proton entry pathway

The N-side proton entry pathway is not yet well established [7]. From the networks drawn in Fig. 2(b), clusters 2 and 3 have residues exposed to the N-side of the protein. The surface residues 4(Glu51), 4(Glu216) and Arg307 (Table 1) are in cluster 2, while 4(Thr27), 4(His58), 4(Tyr61), 7(Ser46), 7(Asn48), 7(Asp49), 7(Glu53) are in cluster 3. The surface residues are connected to the internal residues in the clusters via water molecules. Analysis of single snapshots shows that cluster 2 is the more likely proton entry than cluster 3 as its connection to the protein interior (cluster 4) are found more often (Table SI.2). Thus, subunits Nqo4 and Nqo8 contribute to N-side entry paths with

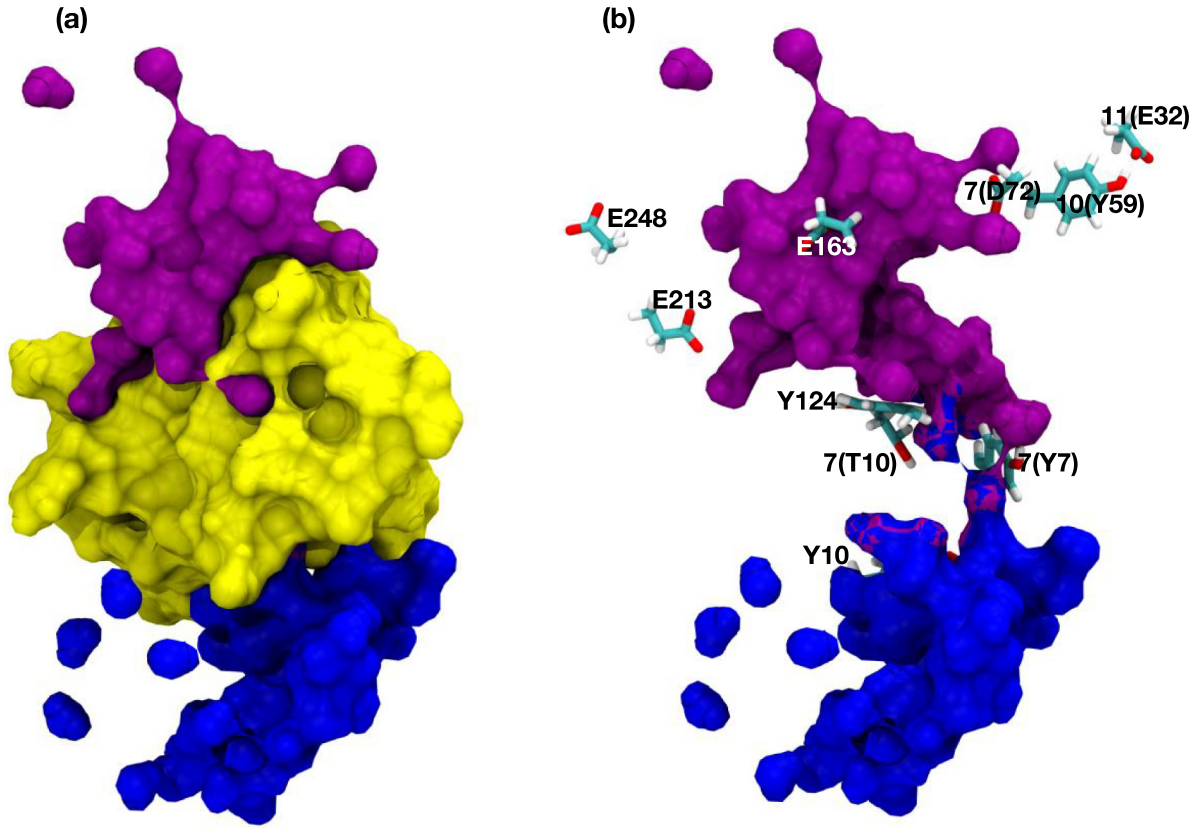

Fig. 3. Representative snapshot from the trajectory with menaquinone bound showing hydrophobic (yellow) and water surface: (purple: waters in central cluster 4, blue: waters in P-side cluster 6); (a) Water and hydrophobic surface; (b) Water surface around 7(T10) and Y124, the two residues that almost bridge the central and the P-side clusters.

possible contributions from subunit Nqo7 in cluster 3.

3.1.2. Proton exit pathway

We see one large cluster of highly hydrogen bonded residues near the P-side of the protein. The surface residues 7(Gln5), Trp3, Tyr10, Lys190, 10(Ser2), 10(Asp118), 10(Gln125), 10(Lys120) are members of cluster 6 (Table 1). Out of these eight surface residues, four are from subunit Nqo10. Thus, subunits Nqo8 and Nqo10 form the path for the proton exit.

3.2. Comparison with MQH_2 and quinone removed structures

The opening and closing of the pathway to the N- and P-side should be coupled to the redox reactions. Here, this may be revealed by comparing the networks in trajectories with different quinone site occupancy and redox state. The MD simulations [41] revealed a difference in hydrogen partners for the Q carbonyls and QH_2 hydroxyls. The hydration and number of hydrogen bonds in the transmembrane domains was also sensitive to the presence or absence of the quinone. Here we trace the effects of the changes in the hydration on the structure of the E-channel.

Comparison of the hydrogen bond network obtained from MCCE analysis of trajectories with MQH_2 bound (Fig. 2c) show similarities, but also significant differences from what is seen in the trajectory with oxidized MQ (Fig. 2a). The MQH_2 hydroxyls most often make hydrogen bonds to D139, E36 and Q226, in cluster 1 (Table SI.2) [41]. These changes reach into the protein, far from the quinone binding site. All clusters are significantly less interconnected. Cluster 3 becomes isolated as its rare connections with clusters 2 and 4 are lost. There is no connection between the N-side cluster 1 and the central cluster 4, as Ser161 has become disconnected from the network (Fig. 2c). This is far different from the rich web of connections found with the quinone present. The break between Cluster 4 and 6 has widened. Interestingly, 7(Thr10) moves from being connected to cluster 4 with MQ present to being connected to cluster 6 while Tyr124 has lost its hydrogen bond connection to either cluster.

The MCCE network analysis of snapshots from the trajectory run with the apo Complex I shows that cluster 3 remains disconnected, but the connections between N-side clusters 1 and 2 and central cluster 4 are being rebuilt (Fig. 2d). What is most notable is the strong increase in connections in the P-side Cluster 6 and the strong connection of Tyr124 and 7(Thr10) within this cluster. These two residues do not bridge the gap between Clusters 4 and 6 in any trajectory, but jump to different sides of the intercluster break under different conditions.

3.3. Overview of the pathway

Our analysis shows the E-pathway to be extended and complex. This complexity has resulted in different ideas for the location of the path. Recent analysis of the E-channel pathway implicated Nqo8 in proton transfer [7,26] but there was no consensus on the role of Nqo10 and Nqo11 [13,19,23] (Fig. SI.9). Here we see Nqo8 forms the spine of the proposed E-channel and residues from this subunit are found in every cluster (Table 1). Nqo4 is involved on the N-side of the protein, Nqo7 and then Nqo10 join the pathway in the middle, while Nqo11 contributes to the cluster on the P-side. The network analysis identifies residues that have been previously implicated in the E-channel and these are given explicit residue labels in Fig. 2a [7,12,13,19,23,25,26,61,62]. However, the network model does not propose a strictly linear path, but rather it identifies a larger group of residues that form clusters where protons can move freely. Hydrophobic regions with low hydration break connections between the

internal clusters 4 and 5 and isolate the P-side cluster 6, as has been reported previously [25,26].

3.4. Adding hydration to complete the connections to the P-side

The main goal is to find the complete pathway from N-side to P-side of the E-channel. The default analysis shows clear connections between the N-side (clusters 1, 2, 3) and the center of the protein (cluster 4) in the MQ containing trajectory. These connections are broken in the snapshots from the trajectory containing MQH_2 and rebuilt in the apo-Complex I trajectory. However, no connections to cluster 5 are ever seen, while those between 4 and 6 involve Tyr124 and 7(Thr10) changing their cluster identity in different states. The region between clusters 4 and 5 or 6 is surrounded by hydrophobic residues (Fig. 3). There are many small cavities, which are dry (Fig. SI.5). Additional calculations were carried out to test the initial conclusions. In particular the goal is to see if water addition can bridge the center of the protein to the P-side.

Seven additional snapshots were analyzed for each quinone state and no connections were seen amongst clusters 4, 5 and 6. In the standard calculations the oxygen positions for waters subjected to GCMC are obtained from the MD snapshot. Additional water positions were added around these clusters using IPECE, which identifies cavities with a radius $\geq$1.4 Å (Fig. SI.10) [52]. These bridge rare connections between residue 7(Asp72) in cluster 4 to residues 10(Tyr59) and 11(Glu32) in cluster 5 in snapshots from the MQ trajectory but not in the MQH_2 or apo structures (Fig. 4a and SI.7). However, despite finding rare connections between cluster 4 and 5, no exit from cluster 5 (via cluster 6 or alternative path) is ever found. The addition of IPECE [52] waters to MC sampling does not change the apparent role of Tyr124 and 7(Thr10) in connecting cluster 4 to 6.

The water content of the trajectory is key to the connections between the clusters. Fig. SI.1 shows the distribution of water counts in each trajectory, and the hydration of analyzed snapshots. Eleven snapshots of an additional trajectory with MQ bound, starting from the same initial conditions, but which became more hydrated was analyzed. The comparison of two trajectories allows us to assess the robustness of our conclusions. The connections amongst the N-side clusters are found to be quite similar to that found in the initial MQ containing trajectory, with interconnections amongst clusters 1, 2, 3 and 4. A few residues shift into or out of the clusters, but in well-connected clusters individual nodes are rarely essential unless they provide a unique connection to another cluster. Cluster 5 remains firmly isolated. However, with the second MQ containing trajectory the connection between clusters 4 and 6 via Tyr124 and 7(Thr10) is now made and 7(Tyr7) in cluster 6 forms an additional connection to Glu130 (Fig. 4b).

3.4.1. Identification of the path to the P-side

The connections between the central cluster 4 and P-side, cluster 6 are the most difficult to find. This area between the two clusters is quite hydrophobic (Fig. 3). However, some connections are seen in the better hydrated trajectory. One is from Glu130 (cluster 4) to 7(Tyr7) (cluster 6). The Glu130 is not highly conserved, being found in only 2% of the sequences (Table SI.6) [55], but the alternatives are Ser or Gly, which may support proton transfers.

Another possible path from cluster 4 to 6 is via Tyr124 and 7(Thr10). These were of interest as they are unusual in being associated with different clusters in the snapshots derived from the MQ and MQH_2 trajectories, providing a sense that they could bridge the two clusters. One concern is that neither residues is well conserved (Table SI.6) [55]. 7(Thr10) is only found in 3% of sequences and more likely to be an Ile or Val. Tyr124 is found 41% of the sequences and is often a Phe (Table SI.6). A covariance analysis was carried out to see if we could identify polar residues that might be found to replace these two residues. No clear candidates were found. Thus, while much of the results provided here for the clusters and their connections involve conserved residues, the connection between 4 and 6 may be unique to a subset of Complex 1 proteins. In addition, 7(Tyr7) and Tyr124 are within 5 Å of each other, indicating that this region of the protein can support several paths between the central and P-exit clusters in this region, which change as water transiently enters hydrophobic channels.

Alternatively, we must acknowledge that the MD trajectories are carried out in a single set of residue protonation states for a limited amount of time. Proton pumps require that pathways are never complete at any given time. Connections must be made a broken in synchrony with the redox reactions in the peripheral region. The regions between 4, 5 and 6 are quite hydrophobic and may require a specific set of triggers to allow connections, which we may not have found.

3.5. Comparison of the pathway presented here with previous E-channel pathways

The hydrogen bond network analysis does not find a unique pathway for proton transfer. It rather sees clusters of interconnected residues that can hold a proton and residues that bridge the gaps

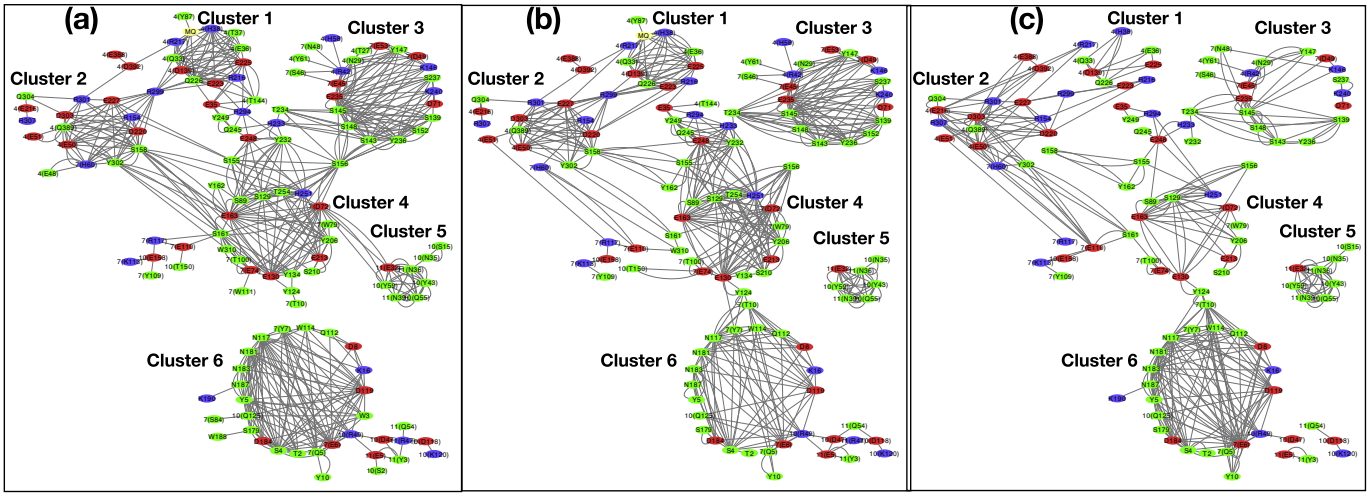

Fig. 4. Hydrogen bond network for trajectory with additional levels of hydration. The node color and position are the same as found in Fig. 2. Here we focus for the connection around cluster 4, cluster 5 and cluster 6 (a) Waters added for GCMC using IPECE [52] in MQ trajectory. (b) Analysis of snapshots from second MQ containing trajectory (c) Analysis of snapshots from wet apo-Complex I trajectory. An enlarged version of these networks is found in Fig. SI.7.

between clusters. The direction of proton transfer through the protein and key residues can be compared with earlier studies of the E-pathway in complex I to see where multiple studies are converging to one answer and where there is still a diversity of views (Fig. SI.9). Inspection of the crystal structure of *T. thermophilus* complex I predicted a pathway from the N-side to the center of the protein mostly involving subunit Nqo8 [7], which was supported by QM/MM-MD calculations [26]. However, these studies did not identify the P-side exit. Other pathways were defined from crystal structure of *E. coli* [19] and *Y. lipolytica* involve Nqo10 and Nqo11, which were supported by MD simulations on the *E. coli* [23] and *T. thermophilus* [25] protein. The N-side portion of the pathway found here generally agrees with those found in earlier studies, running through Nqo8 up to central cluster 4 [7,26]. However, there is the greatest diversity in the proposed P-side exit pathways. One notable difference between the work present here and the previous studies is the role of cluster 5, with the key residues 11(E32) and 10(Y59). In simulations based on any MD snapshot cluster 5 is isolated. We see only rare connections between 7(D72) in cluster 4 and 11(E32) and 10(Y59) in cluster 5 with addition of waters using IPECE [52]. However, cluster 5 is never connected to the P-side surface.

3.6. Proposed pumping cycle

Proton transfer pathways in proton pumps need to have connections, but also gates where connections can be broken. Thus, the network found with MQ bound is well connected on the N-side and appears to be primed for proton uptake. When the quinone is reduced the clusters that connect the E-channel to the N-side become disorganized and disconnected. This will block back flow of the proton. In the structure without quinone the P-side is now highly internally connected and also has many surface connections, which could allow proton release. The network analysis would thus support a model where protons are bound in the MQ state and released in the apo-complex I. The pumping in a semiquinone containing complex I remains a topic for further study.

4. Conclusion

Proton pumping requires connections and gates. The network analysis considers that protons transfer easily within a cluster, finding the sites with the highest proton affinity. Here we identify 6 internally connected clusters. This is similar to what is seen in CcO which has a well-studied Proton Loading Site (PLS) where protons are held during the reaction cycle [6,9]. Thus, the proton may move between several sites in a cluster with facile transfer amongst them shifting as the local proton affinity changes. The clusters are connected by a small number of less connected, bridging residues.

Proton pumping also relies on the connections between clusters being broken to block proton transfer from P- to N-side. We see that the N-side clusters become disconnected in the apo structure when the P-side cluster become better connected. Thus, the system can release protons to the P-side more easily in the apo state. In complex I, the connection between the center of the protein and the P-side is blocked by a layer of hydrophobic residues. More transient connections are seen only in better hydrated trajectory, but this occurs via poorly conserved residues. Thus, this path is used by a subset of complex I proteins.

Declaration of competing interest

The authors declare that they have no known competing financial interests or personal relationships that could have appeared to influence the work reported in this paper.

Acknowledgements

MRG and UK acknowledge funding from National Science Foundation (grant number MCB-1519640). AS acknowledges NSF (MCB-1942763). AS and CG acknowledge start-up funds from the SMS and CASD at Arizona State University, and the resources of the OLCF at the Oak Ridge National Laboratory, which is supported by the Office of Science at DOE under Contract No. DE-AC05-00OR22725, made available via the INCITE program.

Appendix A. Supplementary data

Supplementary data to this article can be found online at https://doi.org/10.1016/j.bbabio.2020.148240.

References

[1] L.A. Sazanov, A giant molecular proton pump: structure and mechanism of respiratory complex I, Nat. Rev. Mol. Cell Biol. 16 (2015) 375–388, https://doi.org/10.1038/nrm3997.
[2] J. Hirst, Mitochondrial complex I, Annu. Rev. Biochem. 82 (2013) 551–575, https://doi.org/10.1146/annurev-biochem-070511-103700.
[3] V.R.I. Kaila, Long-range proton-coupled electron transfer in biological energy conversion: towards mechanistic understanding of respiratory complex I, J. R. Soc. Interface. 15 (2018) 20170916, https://doi.org/10.1098/rsif.2017.0916.
[4] C. Wirth, U. Brandt, C. Hunte, V. Zickermann, Structure and function of mitochondrial complex I, Biochim. Biophys. Acta 1857 (2016) 902–914, https://doi.org/10.1016/j.bbabio.2016.02.013.
[5] T. Ohnishi, Iron-sulfur clusters/semiquinones in complex I, Biochim. Biophys. Acta 1364 (1998) 186–206.
[6] M.R. Gunner, M. Amin, X. Zhu, J. Lu, Molecular mechanisms for generating transmembrane proton gradients, Biochim. Biophys. Acta 1827 (2013) 892–913, https://doi.org/10.1016/j.bbabio.2013.03.001.
[7] R. Baradaran, J.M. Berrisford, G.S. Minhas, L.A. Sazanov, Crystal structure of the entire respiratory complex I, Nature. 494 (2013) 443–448, https://doi.org/10.1038/nature11871.
[8] N. Agmon, The Grotthuss mechanism, Chem. Phys. Lett. 244 (1995) 456–462, https://doi.org/10.1016/0009-2614(95)00905-J.
[9] X. Cai, K. Haider, J. Lu, S. Radic, C.Y. Son, Q. Cui, M.R. Gunner, Network analysis of a proposed exit pathway for protons to the P-side of cytochrome c oxidase, Biochim. Biophys. Acta 1859 (2018) 997–1005, https://doi.org/10.1016/j.bbabio.2018.05.010.
[10] J.E. Walker, The NADH:ubiquinone oxidoreductase (complex I) of respiratory chains, Q. Rev. Biophys. 25 (1992) 253–324.
[11] T. Yagi, A. Matsuno-Yagi, The proton-translocating NADH-quinone oxidoreductase in the respiratory chain: the secret unlocked, Biochemistry. 42 (2003) 2266–2274, https://doi.org/10.1021/bi027158b.
[12] L.A. Sazanov, Respiratory complex I: mechanistic and structural insights provided by the crystal structure of the hydrophilic domain †, Biochemistry. 46 (2007) 2275–2288, https://doi.org/10.1021/bi602508x.
[13] V. Zickermann, C. Wirth, H. Nasiri, K. Siegmund, H. Schwalbe, C. Hunte, U. Brandt, Mechanistic insight from the crystal structure of mitochondrial complex I, Science. 347 (2015) 44, https://doi.org/10.1126/science.1259859.
[14] K. Fiedorczuk, J.A. Letts, G. Degliesposti, K. Kaszuba, M. Skehel, L.A. Sazanov, Atomic structure of the entire mammalian mitochondrial complex I, Nature. 538 (2016) 406–410, https://doi.org/10.1038/nature19794.
[15] R.G. Efremov, R. Baradaran, L.A. Sazanov, The architecture of respiratory complex I, Nature. 465 (2010) 441–445, https://doi.org/10.1038/nature09066.
[16] M. Wikström, V. Sharma, V.R.I. Kaila, J.P. Hosler, G. Hummer, New perspectives on proton pumping in cellular respiration, Chem. Rev. 115 (2015) 2196–2221, https://doi.org/10.1021/cr500448t.
[17] M.O. Ripple, N. Kim, R. Springett, Mammalian complex I pumps 4 protons per 2 electrons at high and physiological proton motive force in living cells, J. Biol. Chem. 288 (2013) 5374–5380, https://doi.org/10.1074/jbc.M112.438945.
[18] A.J.Y. Jones, J.N. Blaza, F. Varghese, J. Hirst, Respiratory complex I in Bos taurus and Paracoccus denitrificans pumps four protons across the membrane for every NADH oxidized, J. Biol. Chem. 292 (2017) 4987–4995, https://doi.org/10.1074/jbc.M116.771899.
[19] R.G. Efremov, L.A. Sazanov, Structure of the membrane domain of respiratory complex I, Nature. 476 (2011) 414–420, https://doi.org/10.1038/nature10330.
[20] M. Narayanan, J.A. Sakyiama, M.M. Elguindy, E. Nakamaru-Ogiso, Roles of subunit NuoL in the proton pumping coupling mechanism of NADH:ubiquinone oxidoreductase (complex I) from Escherichia coli, J. Biochem. 160 (2016) 205–215, https://doi.org/10.1093/jb/mvw027.
[21] J. Michel, J. DeLeon-Rangel, S. Zhu, K.V. Ree, S.B. Vik, Mutagenesis of the L, M, and N subunits of complex I from Escherichia coli indicates a common role in function, PLoS One 6 (2011) e17420, , https://doi.org/10.1371/journal.pone.0017420.
[22] J. Torres-Bacete, E. Nakamaru-Ogiso, A. Matsuno-Yagi, T. Yagi, Characterization of the NuoM (ND4) subunit in Escherichia coli NDH-1 conserved charged residues essential for energy-coupled activities, J. Biol. Chem. 282 (2007) 36914–36922,

https://doi.org/10.1074/jbc.M707855200.
[23] V.R.I. Kaila, M. Wikstrom, G. Hummer, Electrostatics, hydration, and proton transfer dynamics in the membrane domain of respiratory complex I, Proc. Natl. Acad. Sci. U. S. A. 111 (2014) 6988–6993, https://doi.org/10.1073/pnas.1319156111.
[24] P. Tan, Z. Feng, L. Zhang, T. Hou, Y. Li, The mechanism of proton translocation in respiratory complex I from molecular dynamics, J. Recept. Signal Transduct. Res. 35 (2015) 170–179, https://doi.org/10.3109/10799893.2014.942464.
[25] O. Haapanen, V. Sharma, Role of water and protein dynamics in proton pumping by respiratory complex I, Sci. Rep. 7 (2017), https://doi.org/10.1038/s41598-017-07930-1.
[26] A. Di Luca, A.P. Gamiz-Hernandez, V.R.I. Kaila, Symmetry-related proton transfer pathways in respiratory complex I, Proc. Natl. Acad. Sci. U. S. A. 114 (2017) E6314–E6321, https://doi.org/10.1073/pnas.1706278114.
[27] J.C. Fontecilla-Camps, A. Volbeda, C. Cavazza, Y. Nicolet, Structure/function relationships of [NiFe]- and [FeFe]-hydrogenases, Chem. Rev. 107 (2007) 4273–4303, https://doi.org/10.1021/cr050195z.
[28] R.G. Efremov, L.A. Sazanov, The coupling mechanism of respiratory complex I— a structural and evolutionary perspective, Biochim. Biophys. Acta 1817 (2012) 1785–1795, https://doi.org/10.1016/j.bbabio.2012.02.015.
[29] C. Mathiesen, C. Hägerhäll, Transmembrane topology of the NuoL, M and N subunits of NADH:quinone oxidoreductase and their homologues among membrane-bound hydrogenases and bona fide antiporters, Biochim. Biophys. Acta 1556 (2002) 121–132, https://doi.org/10.1016/S0005-2728(02)00343-2.
[30] J. Warnau, V. Sharma, A.P. Gamiz-Hernandez, A.D. Luca, O. Haapanen, I. Vattulainen, M. Wikström, G. Hummer, V.R.I. Kaila, Redox-coupled quinone dynamics in the respiratory complex I, Proc. Natl. Acad. Sci. U. S. A. 115 (2018) E8413–E8420, https://doi.org/10.1073/pnas.1805468115.
[31] O. Haapanen, A. Djurabekova, V. Sharma, Role of second quinone binding site in proton pumping by respiratory complex I, Front. Chem. 7 (2019), https://doi.org/10.3389/fchem.2019.00221.
[32] M.R. Gunner, N.A. Baker, Continuum electrostatics approaches to calculating pK_as and E_ms in proteins, Meth. Enzymol. 578 (2016) 1–20, https://doi.org/10.1016/bs.mie.2016.05.052.
[33] Y. Song, J. Mao, M.R. Gunner, MCCE2: improving protein pK_a calculations with extensive side chain rotamer sampling, J. Comput. Chem. 30 (2009) 2231–2247, https://doi.org/10.1002/jcc.21222.
[34] M. Machuqueiro, A.M. Baptista, Is the prediction of pKa values by constant-pH molecular dynamics being hindered by inherited problems? Proteins. 79 (2011) 3437–3447, https://doi.org/10.1002/prot.23115.
[35] B.K. Radak, C. Chipot, D. Suh, S. Jo, W. Jiang, J.C. Phillips, K. Schulten, B. Roux, Constant-pH molecular dynamics simulations for large biomolecular systems, J. Chem. Theory Comput. 13 (2017) 5933–5944, https://doi.org/10.1021/acs.jctc.7b00875.
[36] J.M. Swails, D.M. York, A.E. Roitberg, Constant pH replica exchange molecular dynamics in explicit solvent using discrete protonation states: implementation, testing, and validation, J. Chem. Theory Comput. 10 (2014) 1341–1352, https://doi.org/10.1021/ct401042b.
[37] Y. Huang, W. Chen, D.L. Dotson, O. Beckstein, J. Shen, Mechanism of pH-dependent activation of the sodium-proton antiporter NhaA, Nat. Commun. 7 (2016) 12940, https://doi.org/10.1038/ncomms12940.
[38] J. Lu, M.R. Gunner, Characterizing the proton loading site in cytochrome c oxidase, Proc. Natl. Acad. Sci. U. S. A. 111 (2014) 12414–12419, https://doi.org/10.1073/pnas.1407187111.
[39] D. Kaur, X. Cai, U. Khaniya, Y. Zhang, J. Mao, M. Mandal, M.R. Gunner, Tracing the pathways of waters and protons in photosystem II and cytochrome c oxidase, Inorganics. 7 (2019) 14, https://doi.org/10.3390/inorganics7020014.
[40] P. Goyal, J. Lu, S. Yang, M.R. Gunner, Q. Cui, Changing hydration level in an internal cavity modulates the proton affinity of a key glutamate in cytochrome c oxidase, Proc. Natl. Acad. Sci. U. S. A. 110 (2013) 18886–18891, https://doi.org/10.1073/pnas.1313908110.
[41] C. Gupta, U. Khaniya, C.K. Chan, F. Dehez, M. Shekhar, M.R. Gunner, L. Sazanov, C. Chipot, A. Singharoy, Charge transfer and chemo-mechanical coupling in respiratory complex I, J. Am. Chem. Soc. (2020), https://doi.org/10.1021/jacs.9b13450.
[42] J.B. Klauda, R.M. Venable, J.A. Freites, J.W. O'Connor, D.J. Tobias, C. Mondragon-Ramirez, I. Vorobyov, A.D. MacKerell, R.W. Pastor, Update of the CHARMM all-atom additive force field for lipids: validation on six lipid types, J. Phys. Chem. B 114 (2010) 7830–7843, https://doi.org/10.1021/jp101759q.
[43] R.B. Best, X. Zhu, J. Shim, P.E.M. Lopes, J. Mittal, M. Feig, A.D. MacKerell, Optimization of the additive CHARMM all-atom protein force field targeting improved sampling of the backbone ϕ, ψ and side-chain χ_1 and χ_2 dihedral angles, J. Chem. Theory Comput. 8 (2012) 3257–3273, https://doi.org/10.1021/ct300400x.
[44] C.H. Chang, K. Kim, Density functional theory calculation of bonding and charge parameters for molecular dynamics studies on [FeFe] hydrogenases, J. Chem. Theory Comput. 5 (2009) 1137–1145, https://doi.org/10.1021/ct800342w.
[45] M.L. Verkhovskaya, N. Belevich, L. Euro, M. Wikström, M.I. Verkhovsky, Real-time electron transfer in respiratory complex I, Proc. Natl. Acad. Sci. U. S. A. 105 (2008) 3763–3767, https://doi.org/10.1073/pnas.0711249105.
[46] H.R. Bridges, E. Bill, J. Hirst, Mössbauer spectroscopy on respiratory complex I: the iron–sulfur cluster ensemble in the NADH-reduced enzyme is partially oxidized, Biochemistry. 51 (2012) 149–158, https://doi.org/10.1021/bi201644x.
[47] M.M. Roessler, M.S. King, A.J. Robinson, F.A. Armstrong, J. Harmer, J. Hirst, Direct assignment of EPR spectra to structurally defined iron-sulfur clusters in complex I by double electron-electron resonance, Proc. Natl. Acad. Sci. U. S. A. 107 (2010), https://ora.ox.ac.uk/objects/uuid:de084bc1-0c02-42f9-8d72-59bd4ae68869 , Accessed date: 1 May 2020.
[48] Y. Zu, S. Di Bernardo, T. Yagi, J. Hirst, Redox properties of the [2Fe-2S] center in the 24 kDa (NQO2) subunit of NADH:ubiquinone oxidoreductase (complex I), Biochemistry. 41 (2002) 10056–10069, https://doi.org/10.1021/bi026026f.
[49] P. Hinchliffe, J. Carroll, L.A. Sazanov, Identification of a novel subunit of respiratory complex I from *Thermus thermophilus*, Biochemistry. 45 (2006) 4413–4420, https://doi.org/10.1021/bi0600998.
[50] P.L. Freddolino, K.H. Gardner, K. Schulten, Signaling mechanisms of LOV domains: new insights from molecular dynamics studies, Photochem. Photobiol. Sci. 12 (2013) 1158–1170, https://doi.org/10.1039/c3pp25400c.
[51] A. Singharoy, I. Teo, R. McGreevy, J.E. Stone, J. Zhao, K. Schulten, Molecular dynamics-based refinement and validation for sub-5 Å cryo-electron microscopy maps, ELife 5 (2016), https://doi.org/10.7554/eLife.16105.
[52] Y. Song, J. Mao, M.R. Gunner, Calculation of proton transfers in Bacteriorhodopsin bR and M intermediates, Biochemistry. 42 (2003) 9875–9888, https://doi.org/10.1021/bi034482d.
[53] Y. Zhang, K. Haider, D. Kaur, V.A. Ngo, X. Cai, J. Mao, U. Khaniya, X. Zhu, S. Noskov, T. Lazaridis, M.R. Gunner, Comparing the water wire in the gramicidin channel obtained with monte carlo sampling with continuum electrostatics or by molecular dynamics with conventional or drude force fields, J. Theor. Comput. Chem. in press (n.d.).
[54] P. Shannon, A. Markiel, O. Ozier, N.S. Baliga, J.T. Wang, D. Ramage, N. Amin, B. Schwikowski, T. Ideker, Cytoscape: a software environment for integrated models of biomolecular interaction networks, Genome Res. 13 (2003) 2498–2504, https://doi.org/10.1101/gr.1239303.
[55] R.P. Joosten, T.A.H. te Beek, E. Krieger, M.L. Hekkelman, R.W.W. Hooft, R. Schneider, C. Sander, G. Vriend, A series of PDB related databases for everyday needs, Nucleic Acids Res. 39 (2011) D411–D419, https://doi.org/10.1093/nar/gkq1105.
[56] X. Cai, C.Y. Son, J. Mao, D. Kaur, Y. Zhang, U. Khaniya, Q. Cui, M.R. Gunner, Identifying the proton loading site cluster in the Ba3 cytochrome c oxidase that loads and traps protons, Biochim. Biophys. Acta. in press (n.d.).
[57] X. Ge, M.R. Gunner, Unraveling the mechanism of proton translocation in the extracellular half-channel of bacteriorhodopsin, Proteins. 84 (2016) 639–654, https://doi.org/10.1002/prot.25013.
[58] J.M. Berrisford, R. Baradaran, L.A. Sazanov, Structure of bacterial respiratory complex I, Biochim. Biophys. Acta 1857 (2016) 892–901, https://doi.org/10.1016/j.bbabio.2016.01.012.
[59] M.A. Tocilescu, U. Fendel, K. Zwicker, S. Dröse, S. Kerscher, U. Brandt, The role of a conserved tyrosine in the 49-kDa subunit of complex I for ubiquinone binding and reduction, Biochim. Biophys. Acta 1797 (2010) 625–632, https://doi.org/10.1016/j.bbabio.2010.01.029.
[60] M.A. Tocilescu, U. Fendel, K. Zwicker, S. Kerscher, U. Brandt, Exploring the ubiquinone binding cavity of respiratory complex I, J. Biol. Chem. 282 (2007) 29514–29520, https://doi.org/10.1074/jbc.M704519200.
[61] P.K. Sinha, J. Torres-Bacete, E. Nakamaru-Ogiso, N. Castro-Guerrero, A. Matsuno-Yagi, T. Yagi, Critical roles of subunit NuoH (ND1) in the assembly of peripheral subunits with the membrane domain of Escherichia coli NDH-1, J. Biol. Chem. 284 (2009) 9814–9823, https://doi.org/10.1074/jbc.M809468200.
[62] V. Sharma, G. Belevich, A.P. Gamiz-Hernandez, T. Róg, I. Vattulainen, M.L. Verkhovskaya, M. Wikström, G. Hummer, V.R.I. Kaila, Redox-induced activation of the proton pump in the respiratory complex I, Proc. Natl. Acad. Sci. U. S. A. 112 (2015) 11571–11576, https://doi.org/10.1073/pnas.1503761112.
[63] A.P. Gamiz-Hernandez, A. Jussupow, M.P. Johansson, V.R.I. Kaila, Terminal electron–proton transfer dynamics in the quinone reduction of respiratory complex I, J. Am. Chem. Soc. 139 (2017) 16282–16288, https://doi.org/10.1021/jacs.7b08486.